Jurnal Kejuruteraan 35(4) 2023: 901-912
https://doi.org/10.17576/jkukm-2023-35(4)-12

An Efficient of Overlapping Grid Method with Scattering Technique in Time Domain for Numerical Modeling

Bong Siaw Wee[a*], Kismet Hong Ping[b] & Shafrida Sahrani[c]

[a]*Department of Electrical Engineering, Politeknik Mukah, 96400 Mukah, Sarawak, Malaysia*
[b]*Department of Electrical and Electronic Engineering, Faculty of Engineering, Universiti Malaysia Sarawak, 94300 Kota Samarahan, Sarawak, Malaysia, Malaysia*
[c]*Institute of IR4.0, Universiti Kebangsaan Malaysia, 43600 Bangi, Selangor Malaysia*

**Corresponding author: shaweibong2016@gmail.com*

Received 6 October 2022, Received in revised form 18 January 2022
Accepted 18 February 2023, Available online 30 July 2023

ABSTRACT

An Overlapping Grid Method (OGM) with Biquadratic Spline Interpolation in scattering technique was developed to solve the direct and inverse scattering issues. A two-dimensional (2D) numerical image model was used to analyze the accuracy of the proposed method in a direct scattering process. It was discovered that when the sub-grid, Δ_{x_s} *increased, the absolute error for the electric field amplitude will also increase. The results also discovered that as the grid size ratio increased, the absolute error of the amplitude* E_Z *will also increase. The findings show that smaller grid spacing and a finer grid size can produce more accurate results. The Overlapping Grid Method (OGM) with Biquadratic Spline Interpolation was expanded by incorporating with Forward-Backward Time Stepping (FBTS) technique to solve inverse scattering issues. Homogenous embedded objects with a square and circular shape are used to validate the efficiency of the proposed method. The findings showed that the proposed numerical method could detect and reconstruct embedded objects in different shapes. The efficiency of the proposed method was examined by Mean Square Error (MSE) and normalizing the functional error. The findings revealed that the MSE of dielectric profiles for the proposed method were lower than the FDTD method in FBTS. The relative permittivity and conductivity profile differed by 27.06% and 20%, respectively. Hence, it was proven that the proposed method successfully solved a known drawback to the FDTD method and produced more accurate and efficient results.*

Keywords: Overlapping Grid Method; Spline Interpolation; scattering technique; object reconstruction

INTRODUCTION

Microwave imaging attracted significant interest among researchers due to its unique features as an excellent diagnostic tool or as a practical resource in several areas. For example, the microwave is primarily used for ground-penetrating radar (Catapano, Gennarelli, Ludeno & Soldovieri 2019; Zhou, Chen, Lyu, & Chen 2022), geophysical exploration (Rosa, Bergmann, & Teixeira, 2020), buried object detection (Wee 2020), and medical diagnostic (Dachena et al. 2020; Stancliff 2017; Salleh et al. 2020).

Active microwave imaging is a wave-based non-invasive imaging method involving two principles; tomographic and confocal radar. Microwave tomography is divided into two categories: qualitative and quantitative imaging. The qualitative microwave imaging method generates a qualitative profile, such as a reflectivity feature or a qualitative picture representing a hidden item. The quantitative imaging approach is used to obtain the electrical and magnetic properties distribution to obtain the geometrical parameters of an imaged object. The spatial distribution of the complex permittivity is calculated using the transmitted (incident) and received (scattered) fields (Nikolova 2011).

The FDTD algorithm is a simple and effective way of addressing Electromagnetic (EM) interaction problems (Baek, Kim, & Jung 2018; Rahman & Rather 2020). Moreover, it can analyse a wide range of frequencies without using additional computer resources. Therefore, the time-domain inversion method is suitable for improving the detection and reconstruction of embedded objects (Narayan 2017; Okada 2014; Schneide 2016). However, this algorithm is limited to intrinsic orthogonal grids due to it is based on a Cartesian coordinate system. Hence, it is challenging to build the meshes for modelling curved borders and microscopic structures (E. Jiménez-Mejía, & Herrera-Murcia, J. 2015; Nilavalan 2002). Several approaches for improving the efficiency of the FDTD method have been published in the literature, including non-uniform (E. Jiménez-Mejía & Herrera-Murcia 2015), sub-gridding (Cabello et al. 2017), and sub-cell algorithm (Navarro et al. 2021). Nevertheless, those approaches still have some disadvantages, such as requiring a long calculation time and additional memory, as well as the Courant-Friedrichs-Lewy (CFL) stability requirement restricting time step or cell size (De Moura & Kubrusly 2013).

Therefore, an Overlapping Grid Method (OGM) with Biquadratic Spline Interpolation in Forward-Backward Time Stepping (FBTS) Technique was proposed and developed in this paper. In order to calculate the dispersed fields for an embedded object, two-dimensional (2D) numerical simulations for electromagnetic (EM) field analysis in various ratios for the sub-grid were carried out. Then, the proposed method incorporated the FBTS inverse scattering technique for detecting and reconstructing embedded objects with different shapes. Finally, the efficiency of the proposed method was examined by Mean Square Error (MSE) and by normalizing the functional error.

METHOD

Overlapping Grid Method (OGM) with Biquadratic Spline Interpolation

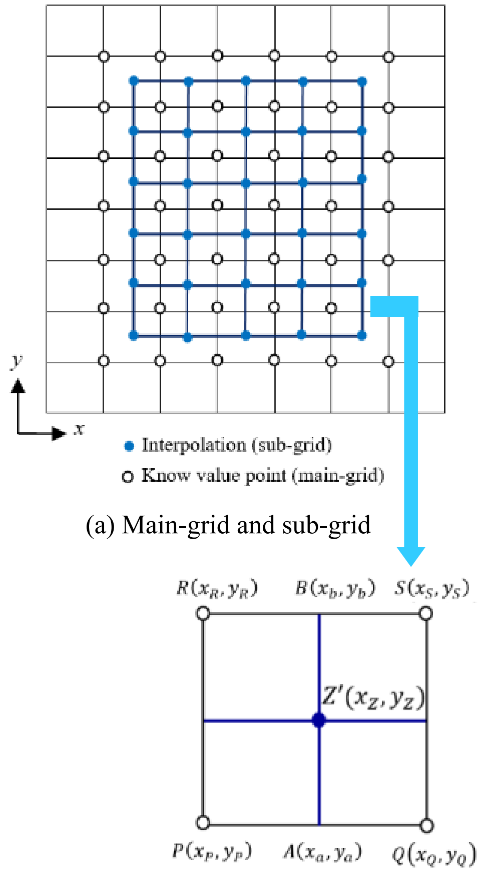

(a) Main-grid and sub-grid

(b) 4-point Biquadratic Spline interpolation

FIGURE 1. Overlapping Grid Method

An Overlapping Grid method is a grid embedding technique that provides a theoretically direct domain decomposition mechanism (Yang, Shao, Li, & Chen 2019). This method divides the computing domain into two or more subdomains in the measured EM region. The advantages of an Overlapping Grid method are it can reduce complex geometric problems and produce the quality and spatial resolution of imaging. An Overlapping grid comprises two grids, as seen in Figure 1(a). The Finite-difference time-domain (FDTD) lattice, also known as Layer 1 (main-grid), is utilized to cover the whole computational domain. Layer 2 (sub-grid) is an overlapping field used to model an undefined numerical entity. The Biquadratic Spline interpolation approach will be used to determine the overlapping region between the main-grid and the sub-grid. The area where the main-grid and sub-grid overlap can be determined by using Biquadratic Spline Interpolation. Then, unknown values at the border points can be retrieved in the overlapping region. Biquadratic Spline interpolation (Boor, 1978; Schumaker, 2015; Späth, 1995) will provide more accurate results due to the fact that it is constructing new data points within the range of a discrete set of known data points (Han 2013; Singh 2016). As a result, it can generate more accurate interpolation for determining curved borders and microscopic features.

Figure 1(b) depicts a four (4) point Biquadratic Spline interpolation derived from Figure 1(a). *P*, *Q*, *R*, and *S* are the four known value points from the main-grid, whereas *Z'* is an unknown value point from the sub-grid. The unknown value of $Z'(x_z, y_z)$ is interpolated by using the $A(x_a, y_a)$ and $B(x_b, y_b)$ at the *y*-axis as in Equation (1).

$$Z' = \left[\frac{D_{j+1} - D_j}{2(y_b - y_a)}\right](y_z - y_a)^2 + d_j(y_z - y_a) + A \tag{1}$$

$$j = 0, 1, 2, \ldots, M$$

where,

$$D_j = 0, \quad D_{j+1} = \frac{2(B - A)}{y_b - y_a} - D_j, \quad j = 0, 1, 2, \ldots, M$$

$$A = \left[\frac{D_{i+1} - D_i}{2(x_Q - x_P)}\right](x_a - x_p)^2 + D_i(x_a - x_P) + P$$

$$\because D_i = 0, \quad D_{i+1} = \frac{2(Q - P)}{x_Q - x_p} - D_i, \quad i = 0, 1, 2, ..., N$$

$$B = \left[\frac{D_{i_2+1} - D_{i_2}}{2(x_s - x_R)}\right](x_b - x_R)^2 + D_{i_2}(x_b - x_R) + R$$

$$\because D_{i_2} = 0, \quad D_{i_2+1} = \frac{2(S - R)}{x_S - x_R} - D_{i_2}, \quad i_2 = 0, 1, 2, \ldots, N$$

DIRECT AND INVERSE SCATTERING TECHNIQUE

There are two types of electromagnetic scattering problems: direct and inverse scattering. The distribution of dispersed fields can be calculated using the direct scattering technique. In contrast, the inverse scattering issue is used to deduce an object's attributes (e.g., structure, location, and dielectric properties) based on scattered field measurement findings.

Direct scattering formulates the problem in the time or frequency domain using microwave signals. As seen in Figure 2, direct scattering is used to calculate an object's dispersed area using two antennas. In free space, the target is implanted with transmitter (T_x) and reception (R_x) antennas inside the Region of Interest (ROI). Each antenna sequentially broadcasts microwave signals, while the remaining antennas act as receivers, absorbing scattered fields.

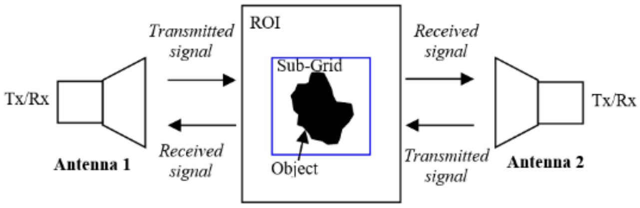

FIGURE 2. Direct scattering

Colton and Kress (Colton 1998) defined the inverse scattering problem as an inverse problem that was highly difficult to solve. However, this scattering problem can be solved by using Forward-Backward Time Stepping (FBTS) technique (Takenaka 2015), as illustrated in Figure 3. The FBTS technique can reconstruct an image based on its electrical characteristics for solving the nonlinear inverse problem.

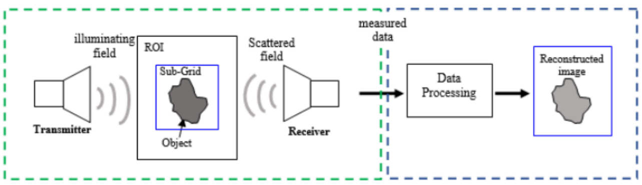

FIGURE 3. FBTS Inverse scattering technique

Microwave tomography collects information about an object by sending microwave pulses and dispersed pulses for data analysis, also known as a computationally intensive image reconstruction algorithm. The overlapping grid method with the FBTS scattering technique is described in detail in (Wee 2020).

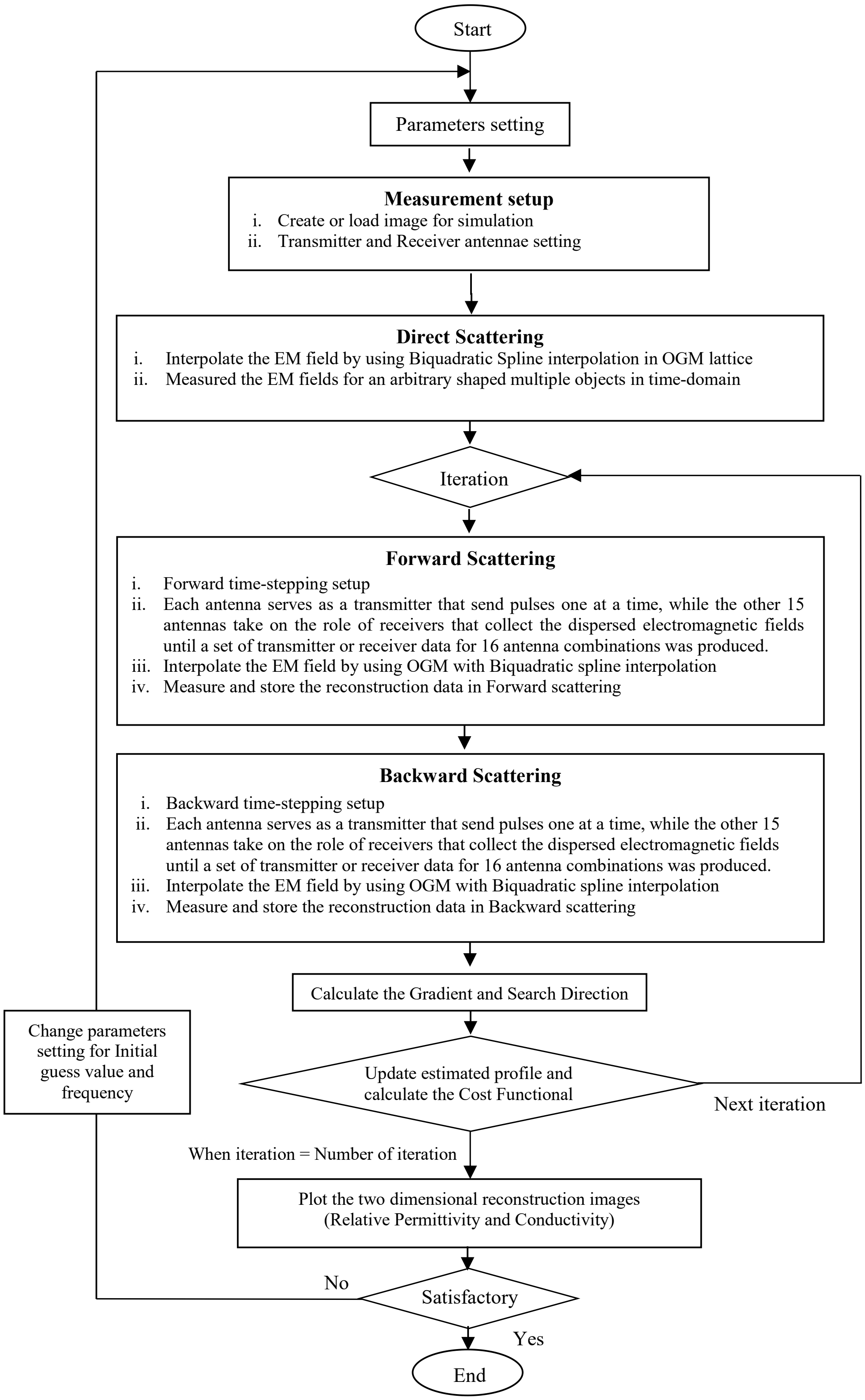

FIGURE 4. Flow chart for proposed numerical method

The OGM with Biquadratic Spline Interpolation in FBTS Inverse Scattering algorithm is shown in Figure 4. All parameters needed for this simulation were specified, and values were assigned. The measuring procedure for the dispersed field was then established. The dielectric characteristics of embedded objects and the Region of Interest (ROI) were included in the actual profiles. In the simulations, an excitation signal was a sinusoidal modulated Gaussian pulse. Each antenna functioned as a transmitter, successively transmitting a pulse, while the remaining 15 antennas served as receivers, collecting dispersed electromagnetic fields.

FBTS is a technique for determining important quantitative information about embedded objects. The forward step begins with applying a Gaussian pulse signal to the predicted profile of an embedded object. Then, the dispersed fields for forwarding time-stepping were calculated by using the OGM approach. In the OGM lattice, the EM field was interpolated using Biquadratic Spline Interpolation for the overlapped region. The forward time-stepping reconstructions data gathered at the receiving location was then compared to the measurement data.

The adjoint fields with backward time-stepping were calculated by using the OGM with Biquadratic Spline Interpolation where there was backward scattering. Data from the receiving point's backward time-stepping reconstructions were gathered and compared to measurement data. Finally, the original profile was irradiated with the difference between the observed and estimated scattered fields as a source.

The cost functional was utilized to reduce the number of FBTS reconstruction iterations. It was calculated by comparing the estimated and actual profiles. Finally, MATLAB was used to illustrate the reconstructed relative permittivity and conductivity images in the two-dimensional. Mean Square Error (MSE) was used to compare the reconstructed image with the original image to evaluate the accuracy of the proposed method.

RESULTS AND DISCUSSION

This paper focuses on the development of the OGM with spline interpolation and demonstrates its efficiency. We have previously published the study related to the noise for the proposed inverse scattering technique in (Elizabeth et al., 2015; Munawwarah Ibrahim et al., 2016). In this research, a study on the performance of OGM with spline interpolation in direct and inverse scattering was evaluated in Case A, Case B and Case C.

CASE A: DIRECT SCATTERING

A 2D numerical model was used to analyse the effectiveness of the OGM with the spline interpolation technique in a direct scattering process. The spline interpolation technique will transfer the data between the main-grid and the sub-grid. Figure 5 shows the sub-grid was configured to converge on top of the main-grid, with L_s and W_s denoting the length and width for sub-grid, respectively. L_m and W_m are the length and width of the main-grid, respectively. The values of L_s, W_s, L_m and W_m were consistent with (i, j) and (m, n). In this study, the sub-grid was set to 50 mm x 50 mm grids, while the main-grid was set to 190 mm x 190 mm grids. In addition, the cell size was set to 1 mm x 1 mm for the main-grid and the sub-grid.

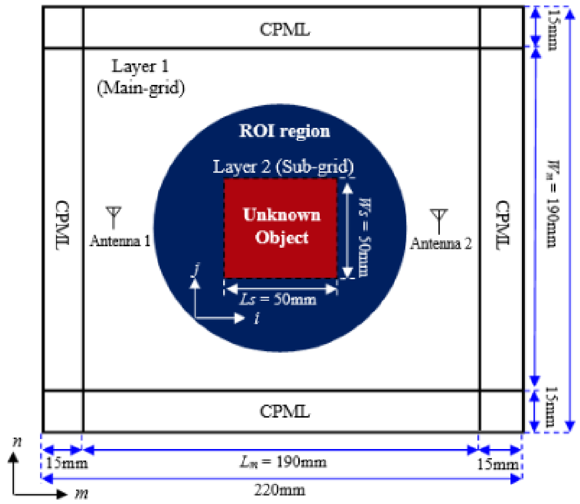

FIGURE 5. The numerical model setup for square object

Two (2) antennas are utilized in this work at a distance of 170 mm. The transmitter antenna will broadcast a signal, while the receiver antenna will collect the dispersed field. The excitation signal was a sinusoidal modulated Gaussian pulse with a core frequency of 2.0 GHz and a bandwidth of 1.3 GHz. This pulse was stimulated into the Overlapping lattice by the transmitter. The main grid was encircled by a Convolution Perfectly Matched Layer (CPML) with a thickness of 15 mm. It is used to eliminate signal reflection at the boundary of the environment. Table 1 presents the dielectric profile setting in free space.

TABLE 1. Dielectric Profiles Setting

Layer	Class	Size	ε_r (F/m)	σ (S/m)
Main-grid	Background	190 mm x 190 mm	1.00	0.00
	ROI Region	50 mm (radius)	1.00	0.00
Sub-grid	Square Object	50 mm x 50 mm	1.00	0.00

CASE A(1): VALIDATION OF ACCURACY BY SPACE INCREMENT OF SUB-GRID WITH A DIRECT SCATTERING

Figure 5 shows the numerical model of the Overlapping method with spline interpolation in free space. The observation point is in the middle of the sub-grid and main-grid. The spaces of main-grid, Δ_{x_m} and Δ_{y_m} were set as $\Delta_{x_m} = \Delta_{y_m} =$ 1 mm. The space of the sub-grid was set as $\Delta_{x_s} = \Delta_{y_s} =$ 1 mm and used as references in this analysis.

The spacing increment of the sub-grid, Δ_{x_s} was changed from 1.2 mm to 2.0 mm to examine an accuracy of the proposed method in direct scattering. However, the Δ_{y_s} was maintained at 1 mm. Figure 6 shows the absolute error of the amplitude of E_Z field versus the space increment of sub-grid, Δ_{x_s} . It was discovered that the absolute error of the amplitude of the E_Z field increased when the Δ_{x_s} increased. As a result, smaller grid spacing or cell sizes have produced more accurate findings.

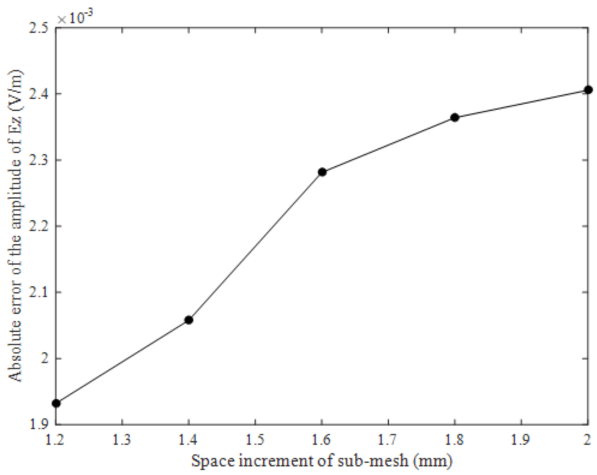

FIGURE 6. The absolute error of the amplitude of E_z field versus space increment of sub-grid

CASE A(2): VALIDATION OF ACCURACY BY RATIO OF THE GRID SIZE WITH DIRECT SCATTERING

A range of ratios of the grid size, R between the main-grid and sub-grid, was utilized to investigate the precision of the proposed numerical method. As shown in Figure 6, the ratios of the grid size among the main grid and the sub-grid were $R = \left(\frac{L_s}{I_s}\right) \Big/ \left(\frac{L_m}{I_m}\right)$. In this analysis, the number of grids on the main grid, $I_{m(m)} \times I_{m(n)}$ were fixed to 190 mm x 190 mm grids. The number of the grids on the sub-grid $I_{s(i)} \times I_{s(j)}$ were set based on Table 2. The number of grids in the sub-grid decreased when the ratio of grid size increased. The ratio of grid size, R = 1.0 and number of the grids $I_{s(i)} \times I_{s(j)} =$ 50 mm x 50 mm for sub-grid were used as a reference in this analysis. All these simulations were carried out in free space.

TABLE 2. The ratio of grid sizes between 0.1 until 0.7

Ratio	Number of grids for sub-mesh, $I_{s(i)} \times I_{s(j)}$ (mm)
0.1	500 x 500
0.2	250 x 250
0.3	166 x 166
0.4	125 x 125
0.5	100 x 100
0.6	83 x 83
0.7	71 x 71

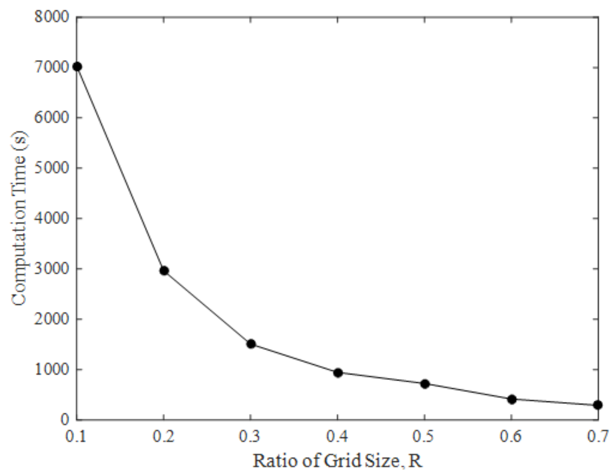

FIGURE 7. The computational time versus the ratio of grid sizes for the sub-grid

Figure 7 illustrates the computing time versus grid size ratio for sub-grid. The computational time decreased when the ratio of grid size increased. The results showed that the smallest grid size ratio required the highest computational time.

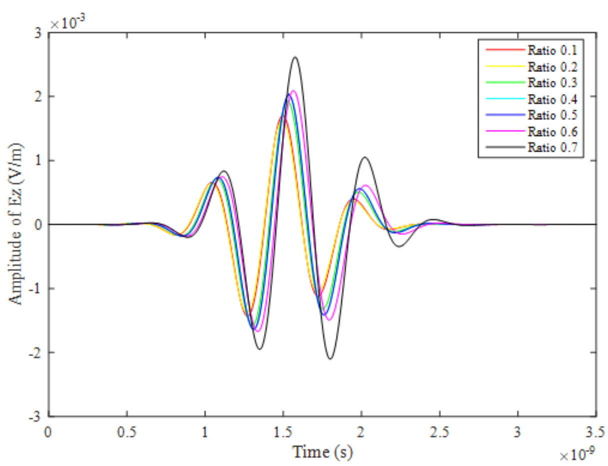

FIGURE 8. The number of steps versus the amplitude of E_z field

Figure 8 shows the amplitude of E_z field with a different ratio of grid size versus the number of steps. The solid line colour (red, yellow, green, cyan, blue, purple, and dark) represented the ratio of the grid, R = 0.1 until 0.7. Figure 9 shows the maximum amplitude of E_z field versus the ratio of grid size. It was found that the maximum amplitude of E_z field increased as the grid size ratio increased.

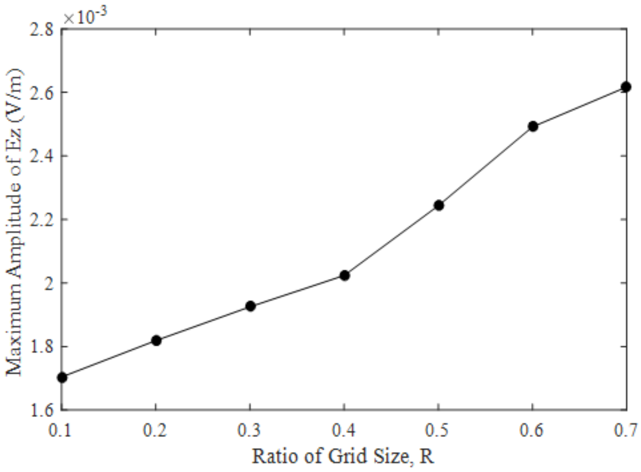

FIGURE 9. The ratio of grid size versus the maximum amplitude of E_z field

The absolute error, $Absolute\ Error = |E_R(t) - E_{R1.0}(t)|$ was used to examine the error analysis for a received signal at the observation point, where $E_{R1.0}(t)$ is an electric field in an overlapping lattice for R=0.1 as the benchmark, and $E_R(t)$ is an electric field in an overlapping lattice for R values ranging from 0.1 to 0.7. Figure 10 depicts the absolute inaccuracy of the amplitude of the E_z field versus the grid size ratio. The findings revealed that as the grid size ratio increased, the absolute error of the amplitude E_z also increased. Consequently, it may be stated that a more refined grid size can yield more accurate findings.

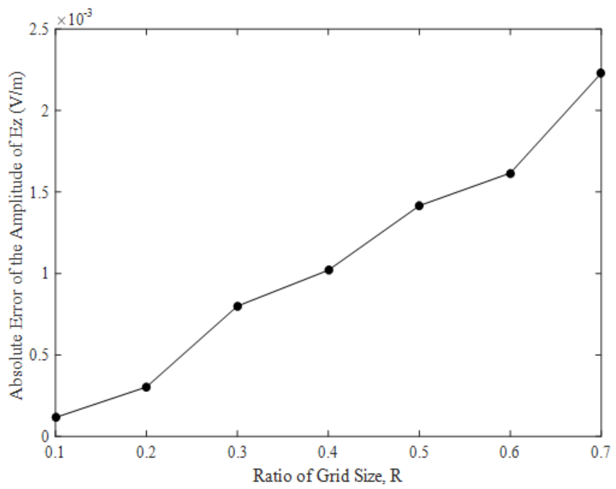

FIGURE 10. The ratio of grid size versus the absolute error of the amplitude of E_z field

CASE B: ANALYSING ELECTROMAGNETIC FIELD FOR AN EMBEDDED OBJECT IN A DIELECTRIC MEDIUM

In case B, the numerical model configuration for an embedded object was created based on Figure 5. The dielectric characteristics were established in accordance with Table 3. The dispersed fields for an embedded object were examined with error analysis to examine the stability and effectiveness of the OGM approach with spline interpolation.

TABLE 3. Dielectric profiles for Case B

Layer	Class	Size	ε_r (F/m)	σ (S/m)
Main-grid	Background	190 mm x 190 mm	1.00	0.00
	ROI Region	50 mm (radius)	9.98	0.18
Sub-grid	Square Object	50 mm x 50 mm	35.26	1.13

The comparison of transmitted and received signals for embedded objects in free space using the FDTD method, OGM with the Bilinear Interpolation, and OGM with the Spline Interpolation is shown in Figures 11 and 12.

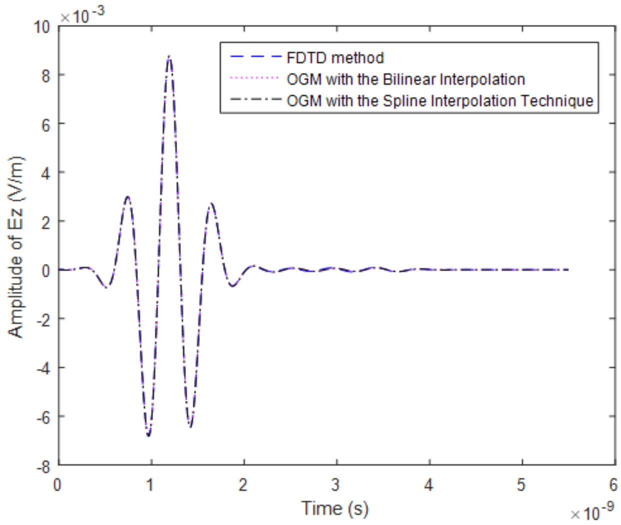

FIGURE 11. Transmitted signal for electric field in Case B

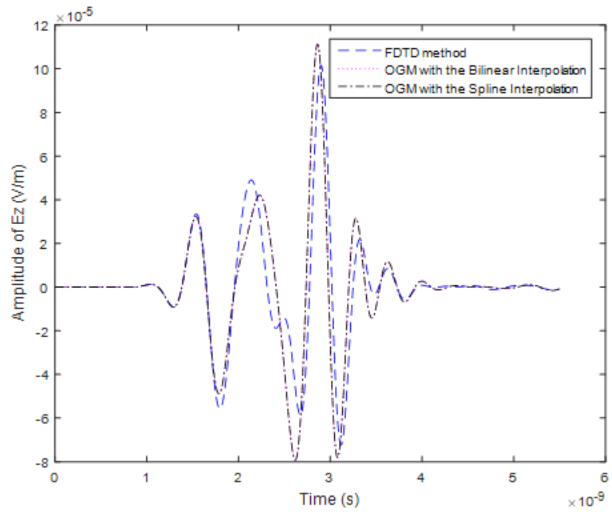

FIGURE 12. Received signal for electric field in Case B

In order to analyze the efficiency of the proposed method, the error analysis for received signal was investigated by using relative error, Relative Error = $\frac{|E_z(t)-E_0(t)|}{E_0(t)}$ and Mean Square Error (MSE), MSE = $\frac{1}{N}\sum_{i=1}^{N}[E_z(t)-E_0(t)]^2$, where, $E_0(t)$ is the electric field in FDTD lattice, $E_z(t)$ is the electric field in OGM with bilinear interpolation or OGM with spline interpolation, and N is the total number of time steps.

TABLE 4. Error analysis for received signal in Case B

	OGM with the bilinear interpolation technique	OGM with the spline interpolation technique
Maximum amplitude peak of E_z (V/m)	1.11278×10^{-4}	1.11269×10^{-4}
Relative error	9.5%	9.49%
MSE	1.8759×10^{-10}	1.87406×10^{-10}

Table 4 presents the error analysis for received signals in free space. The maximum amplitude peak of electric field, $E_0(t)$ for FDTD method was 1.01627×10^{-4} and is used as a reference in this analysis. This is due to the difference between OGM method with bilinear interpolation and OGM method with spline interpolation can be compared and analyzed. The OGM method with spline interpolation showed lower relative error than the OGM method with bilinear interpolation of difference. Besides, the MSE for the OGM method with spline interpolation was also lower than the OGM method bilinear interpolation based on Table 4. Hence, it proves that the OGM method with spline interpolation could to measure the scattered fields around an embedded object accurately as compared with OGM method with bilinear interpolation.

CASE C: RECONSTRUCTION OF EMBEDDED MULTIPLE OBJECTS WITH INVERSE SCATTERING

Figure 13 illustrates the numerical model of microwave tomography for the square object in 2D. Layer 1 was equipped with 190 mm x 190 mm grids. Layer 2 was configured with 50 mm x 50 mm grids. The sub-grid was created as multiple objects and located on top of the main grid with cell size, Δx = 1 mm and Δy = 1 mm. The ROI region was immersed in free space as the backdrop media. A sinusoidal modulated Gaussian pulse with a core frequency of 2.0GHz and a bandwidth of 1.3 GHz was utilized in this work as an excitation signal. The ROI was irradiated by sixteen (16) point source antennas. Each point source antenna served as a transmitter, generating one Gaussian pulse at a time. The remaining fifteen (15) antennas were converted into receivers to collect dispersed fields in the main lattice. Gradient optimization was used up to 100 iterations to reconstruct the microwave image and minimize the functional error.

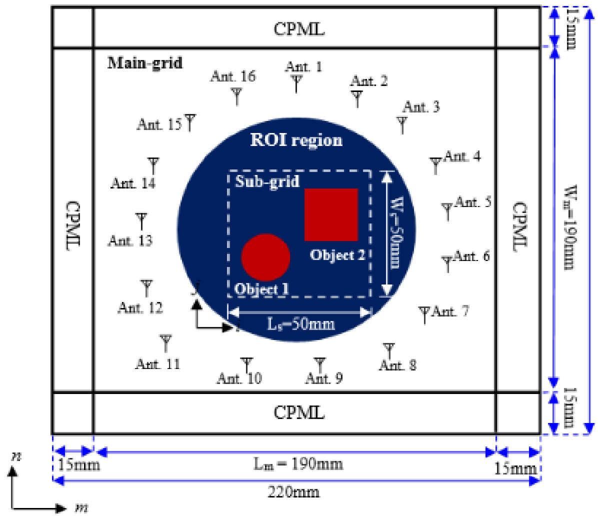

FIGURE 13. The numerical model of multiple embedded objects

The electrical profiles for the numerical model of multiple objects are summarised in Table 5. The dielectric characteristics of ROI represent fatty tissues, and the square object is assumed to represent fibroglandular tissues in the breast. The main-backdrop lattices are supposed to be free space.

TABLE 5. Dielectric Profiles Setting

Layer	Class	Size	ε_r (F/m)	σ (S/m)
Main grid	Background	190 mm x 190 mm	1.00	0.00
Sub-grid	ROI	50 mm (radius)	9.98	0.18
	Circular Object	10 mm (radius)	21.45	0.46
	Square Object	20 mm x 20 mm	21.45	0.46

Figure 14 depicts the real dielectric profiles of multiple simple-shaped objects. Figure 15 demonstrates the reconstructed dielectric profiles of the FDTD method in FBTS and it was used as a reference in this analysis. The FDTD approach in FBTS is limited to intrinsic orthogonal grids because it cannot describe curved borders and minor characteristics of several basic objects. Therefore, an Overlapping Grid Method with scattering technique was proposed in this case study. Figure 16 shows the reconstructed dielectric profiles of the proposed algorithm. The proposed algorithm effectively reconstructed the dielectric profiles of the circular and square objects. The findings present that the proposed algorithm can generate more accurate and efficient interpolation in the reconstruction images to detect curved borders and minor features.

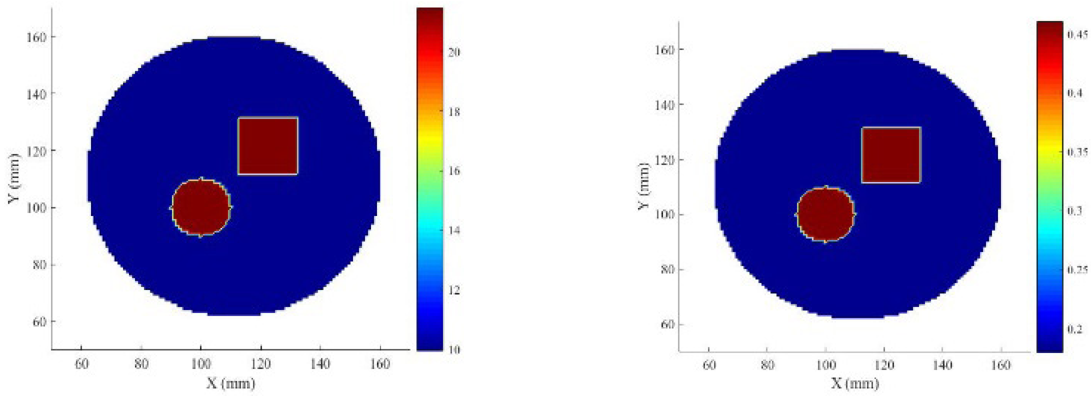

(a) Real relative permittivity

(b) Real conductivity

FIGURE 14. Real dielectric profiles

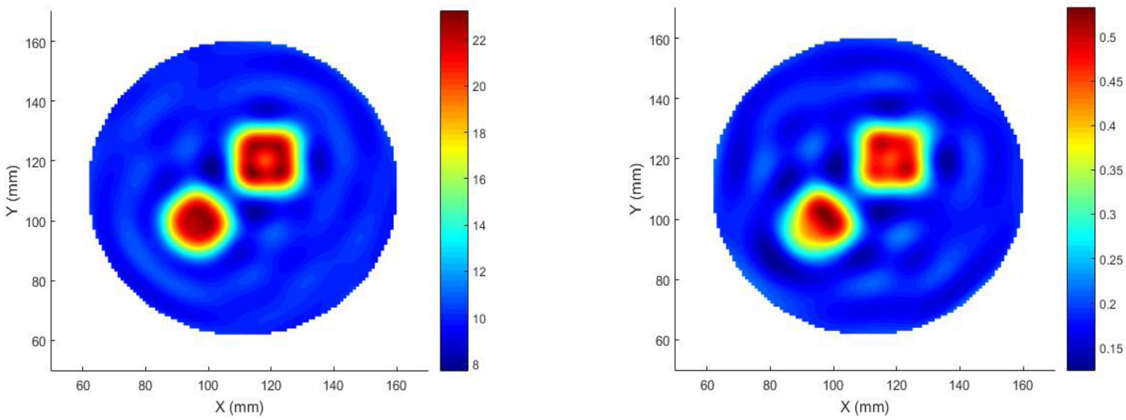

(a) Reconstructed relative permittivity

(b) Reconstructed conductivity

FIGURE 15. Reconstructed dielectric profiles for FDTD method in FBTS

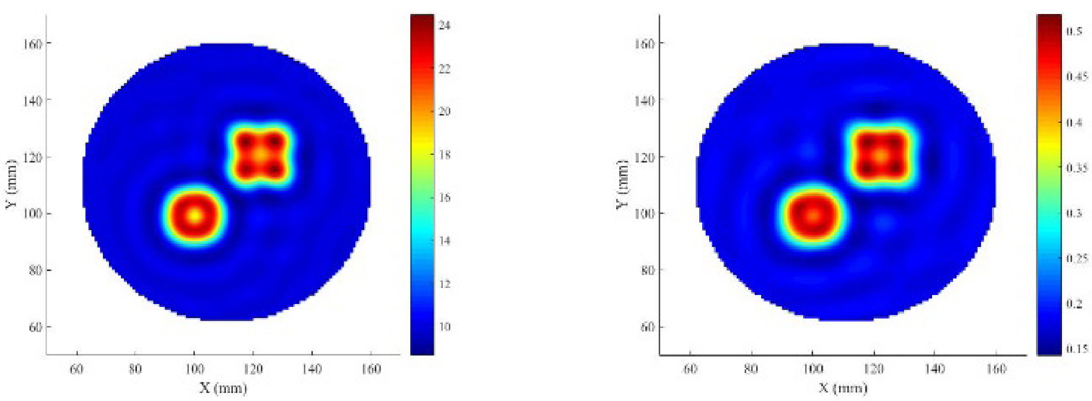

(a) Reconstructed relative permittivity

(b) Reconstructed conductivity

FIGURE 16. Reconstructed dielectric profiles for proposed method

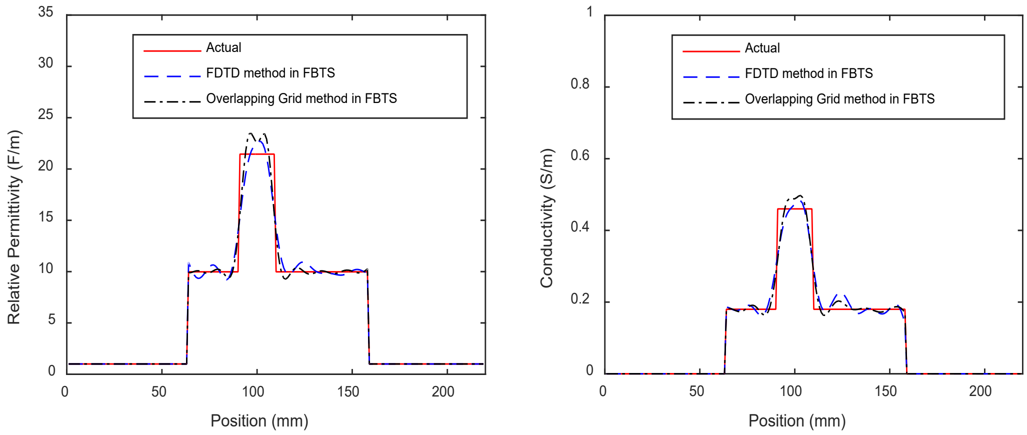

(a) Relative permittivity profile (b) Conductivity profile

FIGURE 17. Cross-sectional view along the x-axis at y =95

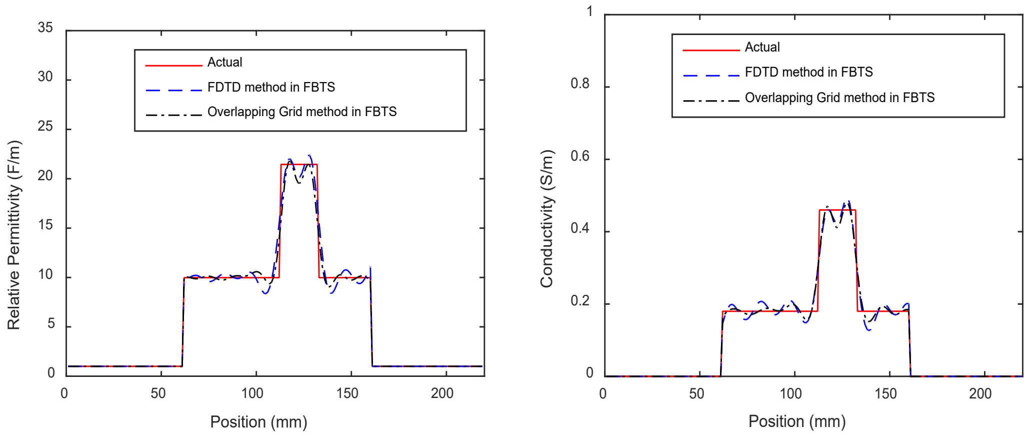

(a) Relative permittivity profile (b) Conductivity profile

FIGURE 18. Cross-sectional view along the x-axis at y =120

Figure 17 and Figure 18 show a 1D cross-section of the original and reconstructed dielectric profiles. Cross-sectional views of the actual and reconstructed dielectric profiles for a circular embedded object are shown in Fig. 15, while for a square embedded object are shown in Fig. 16. These images show the stark difference in dielectric characteristics between the buried items and ROI. The findings demonstrated that the proposed numerical method could distinguish between square and circular objects in ROI while estimating dielectric values accurately.

The proposed method's efficacy was assessed by using the Mean Square Error (MSE), as shown in Table 6. According to this investigation, the MSE of reconstructed dielectric profiles utilizing the proposed method produced much lower values than the FDTD method in FBTS. The relative permittivity profile differed by 27.06%, whereas the conductivity profile differed by 20%.

TABLE 6. MSE of dielectric profiles

Methods	MSE	
	Relative Permittivity Profile	Conductivity Profile
FDTD approach in FBTS	1.6618	9.8572×10^{-4}
Overlapping grid Method with Biquadratic Spline Interpolation in FBTS	1.2120	7.8851×10^{-4}

Figure 19 depicts the normalized functional error vs iterations count. A gradient optimization with 100 iterations was used to reconstruct the numerous simple-shaped objects. As observed, the normalized functional error was reduced as the number of iterations increased. It was also discovered that in FBTS, the OGM with Biquadratic Spline Interpolation showed lower values of normalised functional error than the FDTD approach.

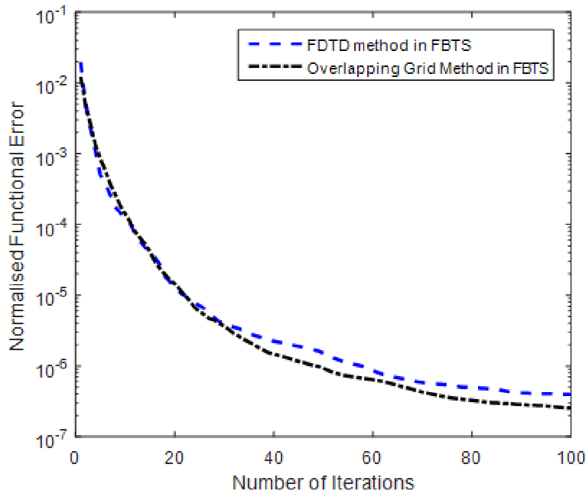

FIGURE 19. Normalized functional error vs iterations count

At 100th iterations, the difference in normalised functional error between these two techniques was 1.41×10^{-7}. Compared to the FDTD approach in FBTS, the results showed that the proposed method could accurately reconstruct numerous simple-shaped objects. Consequently, the proposed method successfully addressed a recognized problem in the FDTD method. It was challenging to simulate the curving borders and tiny features due to inherent orthogonal grid restrictions.

CONCLUSION

An Overlapping Grid Method with Biquadratic Spline Interpolation in direct scattering method was proposed as a new numerical method for measuring the scattered fields around an embedded object. The findings show that smaller grid spacing or cell sizes can produce more accurate results. The results also indicated that when the grid size ratio increases, the absolute error of the amplitude Ez will also be increased. Consequently, it may be stated that a more refined grid size can yield more accurate findings. The FBTS inverse approach was combined with the Overlapping Grid Method with Biquadratic Spline Interpolation to solve inverse scattering issues. The findings demonstrated that the proposed technique was excellent at recognizing buried items and rebuilding them into various forms. The location, shape, and interior content of buried artefacts were determined quantitatively. As opposed to the FDTD method in FBTS, the proposed approach generates sharper and better-reconstructed images.

ACKNOWLEDGEMENT

The authors acknowledge Sarawak Research and Development Council (SRDC) [Grant No.: RDCRG/CAT/2019/19] and Universiti Malaysia Sarawak for financial assistance. The authors also gratefully acknowledge Politeknik Mukah for supporting this project.

DECLARATION OF COMPETING INTEREST

None

REFERENCES

Baek, J. W., Kim, D. K. & Jung, K. Y. 2018. Finite-difference time-domain modeling for electromagnetic wave analysis of human voxel model at millimeter-wave frequencies. *IEEE Access* 7: 3635-3643. DOI:https://doi.org/ 10.1109/ ACCESS.2018.2888584.

Boor, C. D. 1978. *A practical guide to spline*: New York: Springer-Verlag.

Cabello, M. R., Angulo, L. D., Alvarez, J., Flintoft, I. D., Bourke, S., Dawson, J. F. & Garcia, S. G. 2017. A hybrid Crank–Nicolson FDTD subgridding boundary condition for lossy thin-layer modeling. *IEEE Transactions on Microwave Theory and Techniques* 65(5): 1397-1406. DOI:https://doi.org/10.1109/TMTT.2016.2637348.

Catapano, I., Gennarelli, G., Ludeno, G. & Soldovieri, F. 2019. Applying ground-penetrating radar and microwave tomography data processing in cultural heritage: State of the art and future trends. *IEEE Signal processing magazine* 36(4): 53-61. DOI:https://doi.org/10.1109/ MSP.2019.2895121.

Colton, D. & Kress, R. 1998. *Inverse acoustic and electromagnetic scattering theory* (3rd ed.) (Vol. 93). New York: Springer

Dachena, C., Fedeli, A., Fanti, A., Lodi, M. B., Pastorino, M. & Randazzo, A. 2020. Microwave Imaging for the Diagnosis of Cervical Diseases: A Feasibility Analysis. *IEEE Journal of Electromagnetics, RF and Microwaves in Medicine and Biology*. DOI:https://doi.org/10.1109/ JERM.2020.3042711.

De Moura, C. A. & Kubrusly, C. S. 2013. The courant–friedrichs–lewy (cfl) condition. *AMC* 10(12). https:// link.springer.com/ book/10.1007/978-0-8176-8394 8?noAccess=true

Elizabeth, M. A., Ping, K. A. H., Rajaee, N. B., & Moriyama, T. 2015. Chebyshev filter applied to an inversion technique for breast tumour detection. breast, 15(17). https://www.ijret.org/

Han, D. Y. 2013. Comparison of commonly used image interpolation methods. *Paper presented at the Proceedings of the 2nd International Conference on Computer Science and Electronics Engineerings (ICCSEE).*DOI:https://doi.org/10.2991/iccsee.2013.391

Jiménez-Mejía, E. & Herrera-Murcia, J. 2015. Validation of a non-uniform meshing algorithm for the 3D-FDTD method by means of a two-wire crosstalk experimental set-up. *Ingeniería e Investigación* 35: 98-103.

Jiménez-Mejía, E. & Herrera-Murcia, J. 2015. Validation of a non-uniform meshing algorithm for the 3D-FDTD method by means of a two-wire crosstalk experimental set-up. *Ingeniería e Investigación* 35: 98-103.

Munawwarah Ibrahim, P., Hong Ping, K. A., Wei, N. S., Guang, Y., Rajaee, N., & Anyi, M. 2016. Elliptic filter and iterative inversion method for buried object detection applications. In *Applied Mechanics and Materials* (Vol. 833, pp. 164-169). Trans Tech Publications Ltd. https:// www.scientific.net/AMM.833.164.

Narayan, S., Divya, K. M. & Kanth, V. K. 2017. *FDTD modeling of EM field inside microwave cavities*. Singapore: Springer Nature Singapore Pte Ltd. https://link.springer.com/chapter/10.1007/978-981-10-3415-2_1.

Navarro, E. A., Portí, J. A., Salinas, A., Navarro-Modesto, E., Toledo-Redondo, S. & Fornieles, J. 2021. Design & optimization of large Cylindrical Radomes with subcell and non-orthogonal FDTD meshes combined with Genetic Algorithms. *Electronics* 10(18): 2263. DOI:https://doi.org/10.3390/ electronics10182263.

Nikolova, N. K. 2011. Microwave imaging for breast cancer. *IEEE Microwave Magazine* 12(7): 78-94. DOI:https://doi.org/10.1109/MMM. 2011.942702.

Nilavalan, R., Craddock, I. J. & Railton, C. J. 2002. Quantifying numerical dispersion in non-orthogonal FDTD meshes. *IEE Proceedings-Microwaves, Antennas and Propagation* 149(1): 23-27. https://digital-library.theiet.org/content/journals/10.1049/ip-map_20020144.

Okada, N. & Cole, J. B. 2014. Electromagnetic imaging of two-dimensional geometries by multipulse interference using the inverse FDTD method. *Advances in Optical Technologies* 2014: 1-10. DOI:https://doi.org/10.1155/2014/529563.

Rahman, M. M. & Rather, G. 2020. A simple and accurate FDTD based technique to determine equivalent complex permittivity of the multi-layered human tissue in MICS band. *Journal of Science: Advanced Materials and Devices* 5(1): 134-141. DOI:https://doi.org/ 10.1016/j.jsamd.2020.02.004

Rosa, G. S., Bergmann, J. R. & Teixeira, F. L. 2020. Full-wave pseudoanalytical methods for cylindrically symmetric electromagnetic structures: *Applications in sensing and telemetry for geophysical exploration Compendium on Electromagnetic Analysis: From Electrostatics to Photonics: Fundamentals and Applications for Physicists and Engineers Volume 3 Antennas, Antenna Arrays and Microwave Devices, World Scientific*: 385-431. DOI:https://doi.org/10.1142/9789813270305_0010.

Salleh, A., Yang, C. C., Alam, T., Singh, M. S. J., Samsuzzaman, M. & Islam, M. T. 2020. Development of microwave brain stroke imaging system using multiple antipodal vivaldi antennas based on raspberry Pi technology. *J. Kejuruterran*, *32:* 1-6. DOI:https://doi.org/10.17576/jkukm-2020-32(1)-06.

Schneide, J. B. 2016. Understanding the finite-difference time-domain method. *School of electrical engineering and computer science, Washington State University*.

Schumaker, L. L. 2015. Spline functions: Computational methods: *Philadelphia, United Staes of America*: Society for Industrial and Applied Mathematics.

Singh, M. R. & Bhide, A. S. 2016. A review of image retrieval using different types of interpolation techniques. *International Research Journal of Engineering and Technology (IRJET)* 3(12): 1423-1426.

Späth, H. 1995. *Two dimensional spline interpolation algorithms*: Wellesley, United States: AK Peters.

Stancliff, R. 2017. Microwave imaging update: For medical imaging applications. *Paper presented at the 2017 SBMO/IEEE MTT-S International Microwave and Optoelectronics Conference (IMOC). DOI:*https://doi.org/10.1109/IMOC.2017.8121058.

Takenaka, T., Jia, H. & Tanaka, T. 2015. Microwave imaging of electrical property distributions by a Foward-Backward Time-Stepping method. *Journal of Electromagnetic Waves and Applications* 14: 1609-1626.

DOI:https://doi.org/ 10.1163/156939300X00383.

Wee, B. S., Sahrani, S., Ping, K. A. H & Moriyama, T. 2020. Arbitrary Shaped Objects Detection and Reconstruction through Overset Grid Generation Method with B-2-spline Interpolation in Forward-Backward Time-Stepping Inverse Scattering. *Applied Computational Electromagnetic Society Journal* 35(3): 295-304.https://journals.riverpublishers.com/index.php/ACES/article/view/7933.

Yang, D., Shao, F., Li, C. & Chen, H. 2019. Overlapping Grid Technique for Numerical Simulation of a Fast-Cruising Catamaran Fitted with Active T-Foils. *Journal of Marine Science and Application* 18(2): 176-184.https://link.springer.com/article/10.1007/s11804-019-00077-7.

Zhou, X., Chen, Q., Lyu, S. & Chen, H. 2022. Mapping the Buried Cable by Ground Penetrating Radar and Gaussian-Process Regression. *IEEE Transactions on Geoscience and Remote Sensing*: 1-10. DOI:https://doi.org/10.1109/TGRS.2022.3181380.